Backscattering enhancement from a randomly rough surface

Ya-Qiu Jin*
Department of Physics, City College of the City University of New York, New York, New York 10031

Melvin Lax
Department of Physics, City College of the City University of New York, New York, New York 10031
and AT&T Bell Laboratories, Murray Hill, New Jersey 07974-2070

(Received 27 June 1990)

Theoretical evaluation of the angular scattering enhancement around the backscattering direction from a randomly rough surface is studied using the Kirchhoff approach. An analytic formulation of the polarized double-scattered intensity that takes into account the coherence of multiple scattering from the rough surface is used to evaluate quantitatively the scattering enhancement around the backscattering direction from a randomly rough surface.

I. INTRODUCTION

Scattering from a randomly rough surface has been of interest primarily due to its broad application in physics and engineering. Recently, the phenomenon of scattering enhancement around the backscattering direction from a rough surface has attracted attention.[1-5] However, the existing solutions[6,7] to compute the scattering from a rough surface with large slopes are restricted to the single-scattering approximation. The scattering enhancement around the backscattering direction is produced by constructive interference from multiple interactions of the scattered wave with the surface.[8] A few of the methods[9-11] on multiple scattering from a rough surface are largely formal, and do not seem to be tractable yet to assess quantitatively the enhancement effect of multiple scattering. Recently, Monte Carlo calculations have been performed by a number of authors that demonstrate the backscattering enhancement from rough surfaces with large slopes.[12-14] In contrast to our primarily analytical procedure these calculations include multiple-scattering effects by numerical simulation. Tran and Celli[15] have done a simulation that avoids the Kirchhoff approximation.

The object of this paper is to develop an explicit formula to explain and evaluate the scattering enhancement. The polarized scattered power from a randomly rough surface is contributed to by high-order scattered waves as well as single scattered waves. The constructive interference of multiple-scattered waves near the backscattering direction is due to the presence of "time-reversed paths" as illustrated in Fig. 1. This has been pointed out in the discussion of localization phenomena.[16,17] The contribution of this paper is to demonstrate that double scattering is sufficient to demonstrate the coherent angular enhancement. An explicit formula for the polarized bistatic double-scattering coefficient is obtained using an approximate Kirchhoff approach. Although the Kirchhoff approximation is not always valid, the backscattering enhancement obtained in this paper demonstrates that this phenomena is adequately included within the Kirchhoff approximation. Moreover, although more precise quantitative results may require higher-order effects, we demonstrate that the angular enhancement is already explained by double scattering. Double scattering takes account of constructive interference of the scattered waves and is sufficient to yield a quantitative estimate of the angular enhancement from a random dielectric or a highly conducting rough surface.

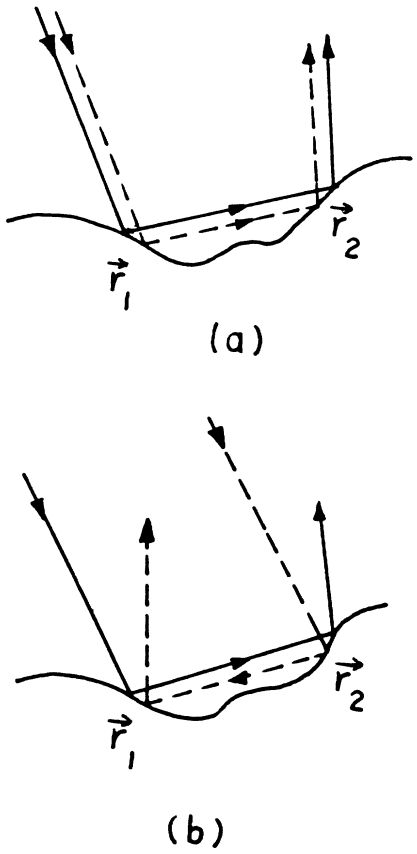

FIG. 1. Double scatterings from coincidental and anticoincidental waves from a roughly rough surface.

II. SINGLE-SCATTERED FIELD

Consider a plane wave incident upon a randomly rough surface. The rough surface is described by the random height $z=\xi(x,y)$. From Huygen's principle, the scattered field $\mathbf{E}_s$ from such a rough surface is written in terms of the actual field $\mathbf{E}$ and incident field $\mathbf{E}_i$ evaluated on the surface:[18]

$$\mathbf{E}_s(\mathbf{r})=\int_A d\mathbf{r}_{1\rho}[i\omega\mu\overleftrightarrow{g}(\mathbf{r},\mathbf{r}_1),\nabla'\times\overleftrightarrow{g}(\mathbf{r},\mathbf{r}_1)]\cdot[\eta\hat{\mathbf{n}}_1\times\mathbf{H}(\mathbf{r}_1),\hat{\mathbf{n}}_1\times\mathbf{E}(\mathbf{r}_1)]^T \tag{1a}$$

$$\equiv\int_A d\mathbf{r}_{1\rho}\overleftrightarrow{G}(\mathbf{r},\mathbf{r}_1)\cdot\overleftrightarrow{R}(\hat{\mathbf{n}}_1,\hat{\mathbf{k}}_s,\hat{\mathbf{k}}_i)\cdot\mathbf{E}_i(\mathbf{r}_1)\ , \tag{1b}$$

where $\eta=\sqrt{\mu_0/\epsilon_0}$ is the impedance of free space, A is the illuminated area, and the free-space dyadic Green's function is

$$\overleftrightarrow{g}(\mathbf{r},\mathbf{r}_1)=\left[\overleftrightarrow{1}+\frac{\nabla\nabla}{k^2}\right]\frac{\exp(ik|\mathbf{r}-\mathbf{r}_1|)}{4\pi|\mathbf{r}-\mathbf{r}_1|}\ . \tag{2a}$$

The normal vector $\hat{\mathbf{n}}_1$ at $\mathbf{r}_1$ is

$$\hat{\mathbf{n}}_1=\frac{-\alpha_x\hat{\mathbf{x}}-\alpha_y\hat{\mathbf{y}}+\hat{\mathbf{z}}}{(1+\alpha_x^2+\alpha_y^2)^{1/2}}\ , \tag{2b}$$

where

$$\alpha_x=\frac{\partial\xi(x,y)}{\partial x},\ \alpha_y=\frac{\partial\xi(x,y)}{\partial y}\ , \tag{2c}$$

and we define

$$\overleftrightarrow{G}(\mathbf{r},\mathbf{r}_1)\equiv[ik\overleftrightarrow{g}(\mathbf{r},\mathbf{r}_1),\nabla\times\overleftrightarrow{g}(\mathbf{r},\mathbf{r}_1)]\ , \tag{3a}$$

$$\overleftrightarrow{R}(\hat{\mathbf{n}}_1,\hat{\mathbf{k}}_s,\hat{\mathbf{k}}_i)\cdot\mathbf{E}_i(\mathbf{r}_1)\equiv[\hat{\mathbf{n}}_1\times\eta\mathbf{H}(\mathbf{r}_1),\hat{\mathbf{n}}_1\times\mathbf{E}(\mathbf{r}_1)]^T\ , \tag{3b}$$

where the superscript T denotes the transpose, the subscript ρ in $d\mathbf{r}_{1\rho}$ denotes the transverse direction, and $\mathbf{E}_i(\mathbf{r}_1)$ denotes the incident field upon $\mathbf{r}_1$. We have replaced $\omega\mu$ in Eq. (1a) by $\omega\mu/\eta=k$ and $\mathbf{H}$ by $\eta\mathbf{H}$ so that the left and right halves of the bidyadic in Eqs. (3a) have the same dimensions, as will the left and right halves of the bivector in Eq. (3b).

In the Kirchhoff approach, the fields at any point on the surface are approximated by the fields that would be present on the local tangent plane at that point. When the implied relation between $\mathbf{E}$ and $\mathbf{E}_i$ is inserted, we have

$$\overleftrightarrow{R}(\hat{\mathbf{n}}_1,\hat{\mathbf{k}}_s,\hat{\mathbf{k}}_i)\equiv[\overleftrightarrow{R}_H,\overleftrightarrow{R}_E]$$
$$=(1+\alpha_x^2+\alpha_y^2)^{1/2}[-(1-R_h)(\hat{\mathbf{n}}_1\cdot\hat{\mathbf{k}}_i)\hat{\mathbf{q}}_i\hat{\mathbf{q}}_i+(1+R_v)(\hat{\mathbf{n}}_1\times\hat{\mathbf{q}}_i)\hat{\mathbf{p}}_i,(1+R_h)(\hat{\mathbf{n}}_1\times\hat{\mathbf{q}}_i)\hat{\mathbf{q}}_i+(1-R_v)(\hat{\mathbf{n}}_1\cdot\hat{\mathbf{k}}_i)\hat{\mathbf{q}}_i\hat{\mathbf{p}}_i]\ , \tag{4}$$

where the local polarization vectors $\hat{\mathbf{q}}_i,\hat{\mathbf{p}}_i$, around $\mathbf{r}_1$ are defined as

$$\hat{\mathbf{q}}_i=\hat{\mathbf{k}}_i\times\hat{\mathbf{n}}_1/|\hat{\mathbf{k}}_i\times\hat{\mathbf{n}}_1|,\ \hat{\mathbf{p}}_i=\hat{\mathbf{q}}_i\times\hat{\mathbf{k}}_i\ . \tag{5}$$

The factor $(1+\alpha_x^2+\alpha_y^2)^{1/2}$, the ratio of the actual area $d\mathbf{r}_{1\rho}$ integrated over to that of the projected area $d\boldsymbol{\rho}_1$ in the x-y plane, has been absorbed into the bidyadic $\overleftrightarrow{R}$. Here R_h,R_v are the local Fresnel reflection coefficients for locally horizontal and vertical polarizations.[18] In the far-field approximation, the dyadic Green's function is

$$\overleftrightarrow{g}(\mathbf{r},\mathbf{r}_1)=\frac{\exp(ikr)}{4\pi r}(\hat{\mathbf{h}}_s\hat{\mathbf{h}}_s+\hat{\mathbf{v}}_s\hat{\mathbf{v}}_s)\exp(-i\mathbf{k}_s\cdot\mathbf{r}_1)\ , \tag{6}$$

where the polarization vectors $\hat{\mathbf{h}}_s,\hat{\mathbf{v}}_s$ associated with the direction of observation, or scattering s, are defined as

$$\hat{\mathbf{h}}_s=\hat{\mathbf{k}}_s\times\hat{\mathbf{z}}/|\hat{\mathbf{k}}_s\times\hat{\mathbf{z}}|,\ \hat{\mathbf{v}}_s=\hat{\mathbf{h}}_s\times\hat{\mathbf{k}}_s\ . \tag{7}$$

Note that for surfaces it is conventional to take $\hat{\mathbf{h}}_s$ as normal to the nominal plane of reflection defined by $\mathbf{k}_s$ and $\hat{\mathbf{z}}$. In the high-frequency limit, the scattered power is principally contributed to by the specular stationary phase points. At a stationary point, the normal vector is determined by the incident and scattering directions as

$$\hat{\mathbf{n}}_{10}=-\frac{\delta\mathbf{k}_0}{|\delta\mathbf{k}_0|}=\frac{-\alpha_{0x}\hat{\mathbf{x}}-\alpha_{0y}\hat{\mathbf{y}}+\hat{\mathbf{z}}}{(1+\alpha_{0x}^2+\alpha_{0y}^2)^{1/2}}\ , \tag{8a}$$

where

$$\delta\mathbf{k}_0\equiv\mathbf{k}_i-\mathbf{k}_s,\ \alpha_{0x}=-\frac{\delta k_{0x}}{\delta k_{0z}},\ \alpha_{0y}=-\frac{\delta k_{0y}}{\delta k_{0z}}\ . \tag{8b}$$

Substituting Eqs. (6) and (8) into Eq. (1), the single-scattered field can be written as

$$\mathbf{E}_s^{(1)}(\mathbf{r})=\int_A d\boldsymbol{\rho}_1\overleftrightarrow{G}(\mathbf{r},\mathbf{r}_1)\cdot\overleftrightarrow{R}(\hat{\mathbf{n}}_1,\hat{\mathbf{k}}_s,\hat{\mathbf{k}}_i)\cdot\mathbf{E}_i^{(0)}(\mathbf{r}_1)$$
$$=\frac{ik\exp(ikr)}{4\pi r}(\hat{\mathbf{h}}_s\hat{\mathbf{h}}_s+\hat{\mathbf{v}}_s\hat{\mathbf{v}}_s)\cdot\overleftrightarrow{R}_0(\hat{\mathbf{k}}_s,\hat{\mathbf{k}}_i)\cdot\hat{\mathbf{e}}_iE_0I\ , \tag{9a}$$

where the properties of the random surface are contained in

$$I=\int_A d\boldsymbol{\rho}_1\exp[i(\mathbf{k}_i-\mathbf{k}_s)\cdot\mathbf{r}_1]\ , \tag{9b}$$

and the incident field is a plane wave:

$$\mathbf{E}_i^{(0)}(\mathbf{r}_1)=\hat{\mathbf{e}}_iE_0\exp(i\mathbf{k}_i\cdot\mathbf{r}_1),\ \hat{\mathbf{e}}_i=\hat{\mathbf{h}}_i\ \text{ or }\ \hat{\mathbf{v}}_i\ . \tag{9c}$$

In the above equations $d\mathbf{r}_{1\rho}$ was replaced by $d\boldsymbol{\rho}_1$ because

the ratio of area elements was absorbed into the reflection coefficient. Thus the integration is now over the nominal flat surface element, although the point $\mathbf{r}_1$ is evaluated on the actual surface.

In obtaining Eq. (9a), we have taken the far-field limit in which $\vec{G}$ can be approximated by

$$\vec{G}(\mathbf{r},\mathbf{r}_1)\approx[ik\vec{\mathbf{g}},\, i\mathbf{k}_s\times\vec{\mathbf{g}}]\approx ik\vec{\mathbf{g}}[\vec{\mathbf{1}},\,\hat{\mathbf{k}}_s\times] \,. \tag{9d}$$

The last step makes explicit use of the asymptotic form of Eq. (6). The scalar product of the two bidyadics can now be written as a product of simple dyadics:

$$\vec{G}(\mathbf{r},\mathbf{r}_1)\cdot\vec{R}(\hat{\mathbf{n}}_1,\hat{\mathbf{k}}_s,\hat{\mathbf{k}}_i)\approx ik\vec{\mathbf{g}}(\mathbf{r},\mathbf{r}_1)\cdot\vec{R}_0(\hat{\mathbf{k}}_s,\hat{\mathbf{k}}_i) \,, \tag{9e}$$

where $\vec{R}_0$ is the ordinary dyadic:

$$\begin{aligned}\vec{R}_0(\hat{\mathbf{k}}_s,\hat{\mathbf{k}}_i)&\equiv\vec{R}_H+\hat{\mathbf{k}}_s\times\vec{R}_E\\&=(1+\alpha_{0x}^2+\alpha_{0y}^2)^{1/2}\{-(1-R_h)(\hat{\mathbf{n}}_{10}\cdot\hat{\mathbf{k}}_i)\hat{\mathbf{q}}_i\hat{\mathbf{q}}_i+(1+R_v)(\hat{\mathbf{n}}_{10}\times\hat{\mathbf{q}}_i)\hat{\mathbf{p}}_i\\&\quad+(1+R_h)[\hat{\mathbf{k}}_s\times(\hat{\mathbf{n}}_{10}\times\hat{\mathbf{q}}_i)]\hat{\mathbf{q}}_i+(1-R_v)(\hat{\mathbf{n}}_{10}\cdot\hat{\mathbf{k}}_i)(\hat{\mathbf{k}}_s\times\hat{\mathbf{q}}_i)\hat{\mathbf{p}}_i\} \,.\end{aligned} \tag{10a}$$

Here Eq. (10a) is obtainable from Eq. (4) by combining magnetic and electric dyadics and inserting the specific directions of Eq. (8).

Since $\vec{R}_0$ is surrounded in Eq. (9a) by factors that retain only the components transverse to $\mathbf{k}_s$ on the left and $\hat{\mathbf{k}}_i$ on the right, the reflection dyadic can be simplified, with the help of Eqs. (7) and (8) to

$$\vec{R}_0=\frac{|\delta\hat{\mathbf{k}}_0|^2}{|\delta\hat{\mathbf{k}}_{0z}|\,|\hat{\mathbf{k}}_s\times\hat{\mathbf{k}}_i|^2}[R_v\hat{\mathbf{k}}_i\hat{\mathbf{k}}_s+R_h(\hat{\mathbf{k}}_s\times\hat{\mathbf{k}}_i)(\hat{\mathbf{k}}_i\times\hat{\mathbf{k}}_s)] \,. \tag{10b}$$

The cancellation of the terms independent of R_h and R_v is a check on our algebra. It is equivalent to the statement that when the reflection coefficients vanish, there is no scattered field. Thus in Eq. (1a) the total fields $\mathbf{H}$ and $\mathbf{E}$ can be replaced by the scattered fields $\mathbf{H}_s$ and $\mathbf{E}_s$, respectively.

The bistatic scattering coefficient of single-scattered power is customarily defined[19] as the scattered power per unit solid angle in the scattering direction $\hat{\mathbf{k}}_s$ multiplied by 4π divided by the intercepted power in direction $\hat{\mathbf{k}}_i$:

$$\gamma_{ba}^{(1)}=\lim_{A\to\infty}\lim_{r\to\infty}\frac{4\pi\langle|\mathbf{E}_{sb}(\mathbf{r})|^2\rangle/(A/r^2)}{\cos\theta_i E_{ia}^2} \,, \tag{11a}$$

where a and b are polarization components. Using Eq. (9a), the squared field can be written as

$$\frac{\langle|\mathbf{E}_{sb}^{(1)}(\mathbf{r})|^2\rangle}{\mathbf{E}_{ia}^2}=\frac{k^2}{16\pi^2r^2}|\mathbf{b}\cdot\vec{R}_0\cdot\mathbf{a}|^2\langle|I|^2\rangle \,. \tag{11b}$$

By using stationary phase methods, it is easy to show[18] that

$$\frac{\langle|I|^2\rangle}{A}=\frac{(2\pi)^2}{(\delta k_{0z})^2}p_2(\alpha_{0x},\alpha_{0y}) \,, \tag{11c}$$

where the components of α_0 are given in Eq. (8b). Thus we can write

$$\langle|\mathbf{E}_s^{(1)}(\mathbf{r})|^2\rangle=\frac{Ak^2E_0^2}{4r^2\delta k_{0z}^2}|\mathbf{F}^{(0)}(\hat{\mathbf{k}}_s,\hat{\mathbf{k}}_i)|^2p_2(\alpha_{0x},\alpha_{0y}) \tag{11d}$$

and

$$\gamma_{ba}^{(1)}=\frac{k^2}{16\pi\cos\theta_i}|\mathbf{b}\cdot\vec{R}_0\cdot\mathbf{a}|^2\frac{\langle|I|^2\rangle}{A} \,, \tag{11e}$$

where $p_2(\alpha_{0x},\alpha_{0y})$ is the probability density function of the slope at the stationary points, $\mathbf{F}_{ba}^{(0)}=\mathbf{b}\cdot\vec{R}_0\cdot\mathbf{a}$ and the functions $\mathbf{F}_{ba}^{(0)}$ are given in Appendix A. The subscripts of the function F, $ba\,(a,b=h$ or $v)$, denote the a-polarized incident and the b-polarized scattered fields. Equation (11d) can be simply multiplied by a shadowing function[7,20] $S(\hat{\mathbf{k}}_i,\hat{\mathbf{k}}_s)$ to take into account the shadowing effect associated with the incident and scattered rays $\hat{\mathbf{k}}_i,\hat{\mathbf{k}}_s$. Our numerical calculations will make use of a convenient analytical approximation to the shadowing function developed by Wagner.[21] We note that a debate between Brockelman and Hagfors[22] and Beckmann[23] was, according to Sancer,[20] resolved by Wagner[21] and Smith.[24] Briefly, Brockelman and Hagfors[22] argued that the traditional shadowing function $S(\mathbf{k}_s,\mathbf{k}_i)$, which describes the probability that an average point of the surface will not lie in shadow for light with the given incident and scattering directions, must be replaced by a new shadowing function $R(\mathbf{k}_s,\mathbf{k}_i)$ that performs an average conditional on the local slope being perpendicular to the incident beam. (They were interested in backscattering only.) In our language, in the general case, the slope of the surface must be such that the point is a stationary point, that is, such that a plane mirror with that slope would reflect the incident beam into the scattered beam direction. This is patently true, and has been verified by comparison of computer experiments of Brockelman and Hagfors[22] with the analytical approximations of Wagner[21] and Smith.[24] To the extent that our procedure selects the points of stationary phase during the evaluation of the spatial integrals, it automatically provides the weighting desired by Brockelman and Hagfors.[22]

Single-scattering results are not new but are displayed in Fig. 2 for three incident angles. Figure 3 shows the effects of shadowing at an incident angle of 40°.

III. DOUBLE-SCATTERING FIELDS

For double-scattering depicted in Fig. 1, the scattered power is contributed by those sequentially scattering waves at $\mathbf{r}_1,\mathbf{r}_2$ that undergo the reincident (on $\mathbf{r}_2$) and rebounced (from $\mathbf{r}_1$) scatterings. Taking the single-scattered field from $\mathbf{r}_1$ in a specular direction $\hat{\mathbf{k}}_1$ as the incident one upon $\mathbf{r}_2$, the double-scattered field can be written as

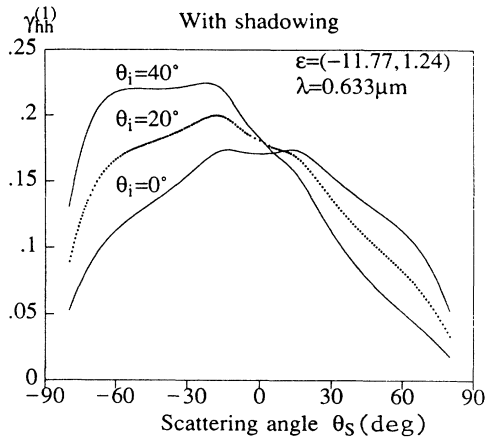

FIG. 2. Single scattering vs scattering angle for incident angles: $\theta_i=40°$, 20°, and 0°, for both $\phi_s=180°$ and 0°. Results for $\phi_s=180°$ are plotted as negative θ_s. In all cases we choose $\phi_i=0°$. All calculations were done using shadowing like that of Wagner (Ref. 21). Parameters are rms height fluctuation $\sigma=2$ μm, correlation length $l=1.7$ μm, wavelength $\lambda=0.633$ μm, and dielectric constant $\epsilon=(-11.77+i1.24)\epsilon_0$.

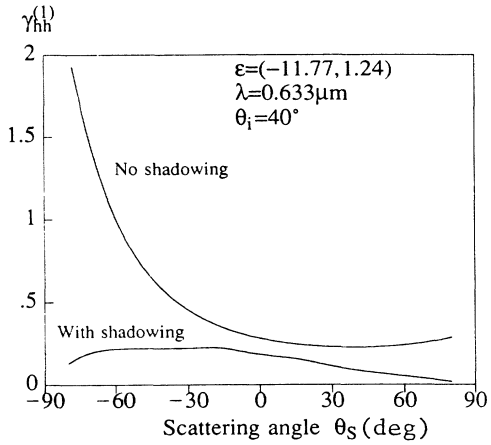

FIG. 3. Effect of shadowing on single scattering. Parameters are rms height fluctuation $\sigma=2$ μm, correlation length $l=1.7$ μm, wavelength $\lambda=0.633$ μm, dielectric constant $\epsilon=(-11.77+i1.24)\epsilon_0$, and incident angles 40°. A comparison is made with and without Wagner shadowing.

$$\mathbf{E}_s^{(2)}(\mathbf{r})=\int_A d\boldsymbol{\rho}_2\int_A d\boldsymbol{\rho}_1\vec{\mathbf{G}}(\mathbf{r},\mathbf{r}_2)\cdot\vec{\mathbf{R}}(\hat{\mathbf{n}}_2,\hat{\mathbf{k}}_s,\hat{\mathbf{k}}_1)\cdot\vec{\mathbf{G}}(\mathbf{r}_2,\mathbf{r}_1)\cdot\vec{\mathbf{R}}(\hat{\mathbf{n}}_1,\hat{\mathbf{k}}_1,\hat{\mathbf{k}}_i)\cdot\mathbf{E}_i^{(0)}(\mathbf{r}_1)\ . \tag{12}$$

It is assumed that the scattering intensity is only contributed to by correlated closely located points. (In other words, the dashed lines in Fig. 1 for scattering from adjacent points are assumed infinitesimally close to the solid lines.) Then the scattered intensity depicted in Figs. 1(a) and 1(b) is approximately written as

$$\begin{aligned}&\langle|\mathbf{E}_s^{(2)}(\mathbf{r})|^2\rangle S^2\int_A d\boldsymbol{\rho}_2\int_A d\boldsymbol{\rho}_1\langle|\vec{\mathbf{G}}(\mathbf{r},\mathbf{r}_2)\cdot\vec{\mathbf{R}}(\hat{\mathbf{n}}_2,\hat{\mathbf{k}}_s,\hat{\mathbf{k}}_1)\cdot\vec{\mathbf{G}}(\mathbf{r}_2,\mathbf{r}_1)\cdot\vec{\mathbf{R}}(\hat{\mathbf{n}}_1,\hat{\mathbf{k}}_1,\hat{\mathbf{k}}_i)\cdot\mathbf{E}_i^{(0)}(\mathbf{r}_1)|^2\rangle\\&+S^2\Big\langle\int_A d\boldsymbol{\rho}_2\int_A d\boldsymbol{\rho}_1\vec{\mathbf{G}}(\mathbf{r},\mathbf{r}_2)\cdot\vec{\mathbf{R}}(\hat{\mathbf{n}}_2,\hat{\mathbf{k}}_s,\hat{\mathbf{k}}_1)\cdot\vec{\mathbf{G}}(\mathbf{r}_2,\mathbf{r}_1)\cdot\vec{\mathbf{R}}(\hat{\mathbf{n}}_1,\hat{\mathbf{k}}_1,\hat{\mathbf{k}}_i)\cdot\mathbf{E}_i^{(0)}(\mathbf{r}_1)\\&\cdot\vec{\mathbf{G}}^*(\mathbf{r},\mathbf{r}_1)\cdot\vec{\mathbf{R}}^*(\hat{\mathbf{n}}_1,\hat{\mathbf{k}}_s,\hat{\mathbf{k}}_1')\cdot\vec{\mathbf{G}}^*(\mathbf{r}_1,\mathbf{r}_2)\cdot\vec{\mathbf{R}}^*(\hat{\mathbf{n}}_2,\hat{\mathbf{k}}_1',\hat{\mathbf{k}}_i)\cdot\mathbf{E}_i^{(0)*}(\mathbf{r}_2)\Big\rangle=\langle|\mathbf{E}_s^{(2+)}(\mathbf{r})|^2\rangle+\langle|\mathbf{E}_s^{(2-)}(\mathbf{r})|^2\rangle\ ,\end{aligned} \tag{13a}$$

where S is an area to be discussed below. The first average (denoted by the superscript + in later equations) is contributed to by the coincident waves [Fig. 1(a)], and the second one (denoted below by the superscript −) is by the anticoincident waves [Fig. 1(b)]. This is similar to the analysis of the ladder and cross terms in Feynman diagrams.[25] The second average becomes smaller as the observation direction moves away from the backscattering direction and increases to the same value as the first one at the exact backscattering direction. Thus it is guaranteed to yield an angular enhancement around the backscattering direction.

Our approximation reduces an eightfold integral to a fourfold integral. This can be seen if the absolute square of Eq. (12) is written as a product of two fourfold integrals, with the second fourfold integral using the variables $\boldsymbol{\rho}_1'$ and $\boldsymbol{\rho}_2'$. Our procedure is equivalent to introducing a factor

$$S^2\delta(\boldsymbol{\rho}_1-\boldsymbol{\rho}_1')\delta(\boldsymbol{\rho}_2-\boldsymbol{\rho}_2') \tag{13b}$$

into the "direct" term, and a factor

$$S^2\delta(\boldsymbol{\rho}_2-\boldsymbol{\rho}_1')\delta(\boldsymbol{\rho}_1-\boldsymbol{\rho}_2') \tag{13c}$$

into the "crossed" term, where S is the area over which overlapping paths are important. A crude estimate of S is given in Appendix B. A more precise evaluation of S is being investigated using stationary phase procedures. For the moment, then, the two contributions to Eq. (13) have an appropriate relative value but are not assigned an absolute value.

Making use of the two-dimensional Fourier transformation of the Green's function[26] of Eq. (2a), we have

$$\vec{\mathbf{g}}(\mathbf{r},\mathbf{r}_2)=\int d\mathbf{k}_\rho\vec{\mathbf{g}}^{\pm}(\mathbf{k}_\rho,z,z_2)e^{i\mathbf{k}_\rho\cdot(\mathbf{r}_\rho-\mathbf{r}_{2\rho})}\ , \tag{14a}$$

where

$$\vec{\mathbf{g}}^{\pm}(\mathbf{k}_\rho,z,z_2)=\frac{1}{8\pi^2}\frac{1}{k_z}\vec{\mathbf{H}}e^{\pm ik_z(z-z_2)}\ , \tag{14b}$$

where the tensor $\vec{\mathbf{H}}$ projects out the transverse part of the reflection coefficient:

$$\vec{\mathbf{H}}\equiv[\hat{\mathbf{h}}(\pm k_z)\hat{\mathbf{h}}(\pm k_z)+\hat{\mathbf{v}}(\pm k_z)\hat{\mathbf{v}}(\pm k_z)] \tag{14c}$$

and $\pm$ is, respectively, taken corresponding to $z > z_2$ and $z < z_2$, and the two-dimensional integral can be written in spherical coordinates in the form

$$\int d\mathbf{k}_\rho \equiv k^2 \int_0^{\pi/2} d\theta \sin\theta\cos\theta \int_0^{2\pi} d\phi \ .$$

Since multiple scattering from a rough surface is appreciable in the problem of enhancement, the propagation constant of the scattered wave k in (14) should be understood as an effective propagation constant, which is different from that in free space k_0, and is related to the underlying medium and roughness distribution. The imaginary part of k, $k''=\kappa_e/2$, where κ_e is the extinction coefficient. This is similar to the case of multiple scattering from discrete scatterers, where an effective propagation constant was introduced, and related to the dielectric constant and fractional volume of scatterers.[27]

Using Eq. (9e) above, and substituting the Fourier transformations of the Green's functions $\vec{g}(\mathbf{r},\mathbf{r}_2), \vec{g}^{\pm}(\mathbf{r}_2,\mathbf{r}_1)$ into Eq. (13a), and approximating the slopes at $\mathbf{r}_1,\mathbf{r}_2$ with the stationary values, we obtain the first average of (13) as

$$\langle |\mathbf{E}_s^{(2+)}(\mathbf{r})|^2 \rangle = \left\langle \int_A d\boldsymbol{\rho}_2 \int_A d\boldsymbol{\rho}_1 \left| \int d\mathbf{k}_\rho \vec{g}^{+}(\mathbf{k}_\rho, z, z_2) \cdot \exp[i\mathbf{k}_\rho\cdot(\mathbf{r}_\rho - \mathbf{r}_{2\rho})] \cdot \int d\mathbf{k}'_\rho \vec{R}_0(\hat{\mathbf{k}},\hat{\mathbf{k}}')\cdot\vec{g}^{\pm}(\mathbf{k}'_\rho, z_2, z_1) \cdot \exp[i\mathbf{k}'_\rho\cdot(\mathbf{r}_{2\rho}-\mathbf{r}_{1\rho})]\cdot\vec{R}_0(\hat{\mathbf{k}}',\hat{\mathbf{k}}_i)\cdot\hat{\mathbf{e}}_i E_0 \exp(i\mathbf{k}_i\cdot\mathbf{r}_1) \right|^2 \right\rangle \ . \tag{15}$$

In Eq. (15) and subsequent equations, the unknown dimensionless factor S^2k^4 is omitted.

Fung and others[28–30] have shown that if the scattered field intensity can be written in the form

$$\langle |\mathbf{E}_s^{(2+)}(\mathbf{r})|^2 \rangle = \int d\mathbf{k}_\rho f(\mathbf{k}_\rho) |\mathbf{E}_0|^2 \tag{16a}$$

the bistatic cross section can be written in the form

$$\gamma_{pq}^{(2+)}(\hat{\mathbf{k}}_s,\hat{\mathbf{k}}_i) = 4\pi k^2 \cos^2\theta_{0i} f(\mathbf{k}_s) \ . \tag{16b}$$

We can interpret $f(\mathbf{k}_s)$ as the spectrum at $\mathbf{k}_s$ of the electric field fluctuations, normalized to the incident field

$$f(\mathbf{k}_s) = \frac{\langle |E_s^{(2+)}(\mathbf{k}_{\rho s}, z)|^2 \rangle}{E_0^2} \ . \tag{16c}$$

Note that f necessarily has the dimensions of an area, so that the bistatic cross section is dimensionless.

In the scattering direction, $\mathbf{k}_\rho = \mathbf{k}_{\rho s}$. Rewriting $\mathbf{k}'_\rho$ as $\mathbf{k}_\rho$, we obtain

$$\langle |\mathbf{E}_s^{(2+)}(\mathbf{k}_{\rho s}, z)|^2 \rangle = \langle (2\pi)^4 \int d\mathbf{k}_\rho \frac{1}{(8\pi^2)^2 |k_{zs}|^2 |k_z|^2} |\mathbf{F}^{(+)}(\mathbf{k}_s,\mathbf{k},\mathbf{k}_i)|^2 \exp[2(k''_{zs} \mp k''_z) z_2] \exp[-2(k''_{zi} \mp k''_z) z_1] \rangle \ , \tag{17}$$

where $''$ denotes the imaginary part, and the function

$$\mathbf{F}^{(+)}(\mathbf{k}_s,\mathbf{k},\mathbf{k}_i) = [\hat{\mathbf{h}}(k_{sz})\hat{\mathbf{h}}(k_{sz}) + \hat{\mathbf{v}}(k_{sz})\hat{\mathbf{v}}(k_{sz})]\cdot\vec{R}_0(\hat{\mathbf{k}}_s,\hat{\mathbf{k}})\cdot[\hat{\mathbf{h}}(\pm k_z)\hat{\mathbf{h}}(\pm k_z) + \hat{\mathbf{v}}(\pm k_z)\hat{\mathbf{v}}(\pm k_z)]\cdot\vec{R}_0(\hat{\mathbf{k}},\hat{\mathbf{k}}_i)\cdot\hat{\mathbf{e}}_i E_0 \tag{18a}$$

$$= \begin{cases} F_{hh}^{(+)} = F_{hh}^{(2+)} F_{hh}^{(1+)} + F_{hv}^{(2+)} F_{vh}^{(1+)} \\ F_{vv}^{(+)} = F_{vv}^{(2+)} F_{vv}^{(1+)} + F_{vh}^{(2+)} F_{hv}^{(1+)} \\ F_{hv}^{(+)} = F_{hv}^{(2+)} F_{vv}^{(1+)} + F_{hh}^{(2+)} F_{hv}^{(1+)} \\ F_{vh}^{(+)} = F_{vh}^{(2+)} F_{hh}^{(1+)} + F_{vv}^{(2+)} F_{vh}^{(1+)} \ , \end{cases} \tag{18b}$$

where $F_{pq}^{(2+)}$, $F_{pq}^{(1+)}$ ($p,q = h$ or v) are listed in Appendix A, and $\mathbf{k} = \mathbf{k}_\rho \pm k_z\hat{\mathbf{z}}$.

The scattered field in (17) is contributed to by all statistically distributed pairs of $\mathbf{r}_1,\mathbf{r}_2$, which are illuminated, not obscured, and there is no obstacle between them. Therefore, any shadowing to obscure the incident ray $\hat{\mathbf{k}}_i$, and to intersect the scattered rays $\hat{\mathbf{k}},\hat{\mathbf{k}}_s$ should be taken into account. We formally write this shadowing function[31] as

$$S(\hat{\mathbf{k}}_i,\bar{\boldsymbol{\alpha}}_{10}) S(\hat{\mathbf{k}},\bar{\boldsymbol{\alpha}}_{10},\bar{\boldsymbol{\alpha}}_{20}(\rho)) S(\hat{\mathbf{k}}_s,\bar{\boldsymbol{\alpha}}_{20}) \ , \tag{19a}$$

where $\bar{\boldsymbol{\alpha}}_{10},\bar{\boldsymbol{\alpha}}_{20}$ are the stationary slopes determined by

$$\bar{\boldsymbol{\alpha}}_{10}=-\frac{\mathbf{k}_{i\rho}-\mathbf{k}_{\rho}}{k_{iz}-k_z},\quad \bar{\boldsymbol{\alpha}}_{20}=-\frac{\mathbf{k}_{\rho}-\mathbf{k}_{s\rho}}{k_z-k_{sz}}\ . \tag{19b}$$

This means that $\mathbf{k}=\mathbf{k}_{\rho}\pm k_z\hat{\mathbf{z}}$ can be interpreted (in stationary phase) as a vector from $\mathbf{r}_{1\rho}$ to $\mathbf{r}_{2\rho}$.

Taking the average over all possible $z_2=\xi_2$, $z_1=\xi_1$ on the surface, whose distance $|\mathbf{r}_2-\mathbf{r}_1|=[\rho^2+(\xi_2-\xi_1)^2]^{1/2}$, we obtain

$$\begin{aligned}\langle|\mathbf{E}_s^{(2+)}(\mathbf{k}_{\rho s},z)|^2\rangle=(2\pi)^4\int d\mathbf{k}_{\rho}\frac{1}{(8\pi^2)^2|k_{zs}|^2|k_z|^2}|\mathbf{F}^{(+)}(\mathbf{k}_s,\mathbf{k},\mathbf{k}_i)|^2\\ \times\int_{-\infty}^{\infty}d\xi_1\int_{-\infty}^{\infty}d\xi_2 p_6[\xi_1(0),\xi_2(\bar{\boldsymbol{\rho}}),\bar{\boldsymbol{\alpha}}_{10},\bar{\boldsymbol{\alpha}}_{20}]S(\hat{\mathbf{k}}_i,\bar{\boldsymbol{\alpha}}_{10})S(\hat{\mathbf{k}},\bar{\boldsymbol{\alpha}}_{10},\bar{\boldsymbol{\alpha}}_{20})S(\hat{\mathbf{k}}_s,\bar{\boldsymbol{\alpha}}_{20})\\ \times\exp[2(k_{zs}''\mp k_z'')\xi_2]\exp[-2(k_{zi}''\mp k_z'')\xi_1]\ ,\end{aligned} \tag{20}$$

where $p_6[\xi_1,\xi_2,\bar{\boldsymbol{\alpha}}_{10},\bar{\boldsymbol{\alpha}}_{20}]$ is a two-point joint probability density function for heights and slopes. The implicit dependence on $\boldsymbol{\rho}$ has been removed by replacing $\boldsymbol{\rho}$ by its stationary value, $\bar{\boldsymbol{\rho}}$, in terms of ξ_1, ξ_2, and $\mathbf{k}$. This dependence appears only in $\xi_2(\bar{\boldsymbol{\rho}})$. Equation (20) will be evaluated in the next section.

Now we turn to the second average in (13). We obtain

$$\begin{aligned}\langle|\mathbf{E}_s^{(2-)}(\mathbf{r})|^2\rangle=\Big\langle\int_A d\mathbf{r}_{2\rho}\int_A d\mathbf{r}_{1\rho}\int d\mathbf{k}_{\rho}\overleftrightarrow{\mathbf{g}}^{+}(\mathbf{k}_{\rho},z,z_2)e^{i\mathbf{k}_{\rho}\cdot(\mathbf{r}_{\rho}-\mathbf{r}_{2\rho})}\\ \cdot\int d\mathbf{k}_{\rho}'\overleftrightarrow{\mathbf{R}}_0(\hat{\mathbf{k}},\hat{\mathbf{k}}')\cdot\overleftrightarrow{\mathbf{g}}^{\pm}(\mathbf{k}_{\rho}',z_2,z_1)e^{i\mathbf{k}_{\rho}'\cdot(\mathbf{r}_{2\rho}-\mathbf{r}_{1\rho})}\cdot\overleftrightarrow{\mathbf{R}}_0(\hat{\mathbf{k}}',\hat{\mathbf{k}}_i)\cdot\hat{\mathbf{e}}_i E_0 e^{i\mathbf{k}_i\cdot\mathbf{r}_1}\\ \cdot\int d\boldsymbol{\beta}_{\rho}\overleftrightarrow{\mathbf{g}}^{+*}(\boldsymbol{\beta}_{\rho},z,z_1)e^{-i\boldsymbol{\beta}_{\rho}^{*}\cdot(\mathbf{r}_{\rho}-\mathbf{r}_{1\rho})}\\ \cdot\int d\boldsymbol{\beta}_{\rho}'\cdot\overleftrightarrow{\mathbf{R}}_0^{*}(\boldsymbol{\beta},\boldsymbol{\beta}')\cdot\overleftrightarrow{\mathbf{g}}^{\pm *}(\boldsymbol{\beta}_{\rho}',z_1,z_2)e^{-i\boldsymbol{\beta}_{\rho}'^{*}\cdot(\mathbf{r}_{1\rho}-\mathbf{r}_{2\rho})}\cdot\overleftrightarrow{\mathbf{R}}_0^{*}(\hat{\boldsymbol{\beta}}',\hat{\mathbf{k}}_i)\cdot\hat{\mathbf{e}}_i E_0 e^{-i\mathbf{k}_i'^{*}\cdot\mathbf{r}_2}\Big\rangle\ .\end{aligned} \tag{21}$$

Taking $\mathbf{k}_{\rho}=\mathbf{k}_{\rho s}$, and rewriting $\mathbf{k}_{\rho}'$ as $\mathbf{k}_{\rho}$, we readily find

$$\begin{aligned}\langle|\mathbf{E}^{(2-)}(\mathbf{k}_{\rho s},z)|^2\rangle=\langle(2\pi)^4\int d\mathbf{k}_{\rho}\overleftrightarrow{\mathbf{g}}^{+}(\mathbf{k}_{\rho s},z,z_2)e^{-i\mathbf{k}_{\rho s}\cdot\mathbf{r}_{2\rho}}\cdot\overleftrightarrow{\mathbf{R}}_0(\hat{\mathbf{k}}_s,\hat{\mathbf{k}})\cdot\overleftrightarrow{\mathbf{g}}^{\pm}(\mathbf{k}_{\rho},z_2,z_1)e^{i\mathbf{k}_{\rho}\cdot(\mathbf{r}_{2\rho}-\mathbf{r}_{1\rho})}\cdot\overleftrightarrow{\mathbf{R}}_0(\hat{\mathbf{k}},\hat{\mathbf{k}}_i)\cdot\hat{\mathbf{e}}_i E_0 e^{i\mathbf{k}_i\cdot\mathbf{r}_1}\\ \cdot\overleftrightarrow{\mathbf{g}}^{+*}(\mathbf{k}_{\rho s},z,z_1)e^{i\mathbf{k}_{\rho s}^{*}\cdot\mathbf{r}_{1\rho}}\cdot\overleftrightarrow{\mathbf{R}}_0^{*}(\hat{\mathbf{k}}_s,\hat{\mathbf{k}}_1)\cdot\overleftrightarrow{\mathbf{g}}^{\pm *}(\mathbf{k}_{1\rho},z_1,z_2)e^{-i\mathbf{k}_{1\rho}^{*}\cdot(\mathbf{r}_{1\rho}-\mathbf{r}_{2\rho})}\cdot\overleftrightarrow{\mathbf{R}}_0^{*}(\hat{\mathbf{k}}_1,\hat{\mathbf{k}}_i)\cdot\hat{\mathbf{e}}_i E_0 e^{-i\mathbf{k}_i^{*}\cdot\mathbf{r}_2}\rangle\ ,\end{aligned} \tag{22a}$$

where

$$\mathbf{k}_1\equiv\mathbf{k}_i+\mathbf{k}_s-\mathbf{k}\ . \tag{22b}$$

Substituting the Fourier transformations of the Green's functions shown in (14) into (22a), and averaging over all possible $z_1=\xi_1$, $z_2=\xi_2$, and taking account of all shadowing effects, we obtain, similarly to (20), that

$$\begin{aligned}\langle|\mathbf{E}_s^{(2-)}(\mathbf{k}_{\rho s},z)|^2\rangle=(2\pi)^4\int d\mathbf{k}_{\rho}\frac{1}{(8\pi^2)^2|k_{zs}|^2|k_z|^2}\mathbf{F}^{(+)}(\mathbf{k}_s,\mathbf{k},\mathbf{k}_i)\mathbf{F}^{(-)*}(\mathbf{k}_s,\mathbf{k}_1,\mathbf{k}_i)\\ \times\int_{-\infty}^{\infty}d\xi_1\int_{-\infty}^{\infty}d\xi_2 p_6[\xi_1(0),\xi_2(\bar{\boldsymbol{\rho}}),\bar{\boldsymbol{\alpha}}_{10},\bar{\boldsymbol{\alpha}}_{20}]S(\hat{\mathbf{k}}_i,\bar{\boldsymbol{\alpha}}_{10})S(\hat{\mathbf{k}},\bar{\boldsymbol{\alpha}}_{10},\bar{\boldsymbol{\alpha}}_{20})S(\hat{\mathbf{k}}_s,\bar{\boldsymbol{\alpha}}_{20})\\ \times\exp\{2[k_{2z}''\mp k_z''\mp i(k_{zs}'+k_{zi}')]\xi_2\}\exp\{-2[k_{zi}''\mp k_z''\mp i(k_{zs}'+k_{zi}')]\xi_1\}\ ,\end{aligned} \tag{23}$$

where $'$ denotes the real part, $\pm$ denotes $z_2>z_1$ and $z_2<z_1$, respectively, and the function $\mathbf{F}^{(-)}$ is defined in Appendix A in a similar way as $\mathbf{F}^{(+)}$ in Eq. (18). Thus the bistatic scattering coefficient due to the second average in Eq. (13) can be obtained as in Eq. (16b):

$$\gamma_{pq}^{(2-)}(\hat{\mathbf{k}}_s,\hat{\mathbf{k}}_i)=4\pi k_0^2\cos^2\theta_i\frac{\langle|E_{sp}^{(2-)}(\mathbf{k}_{\rho s},z)|^2\rangle}{E_{0q}^2}\ . \tag{24}$$

IV. ANGULAR SCATTERING ENHANCEMENT

Comparing Eq. (23) with Eq. (20), it is easy to see that Eq. (23) follows from Eq. (20) by replacing k_z'' by $k_z'+i\Delta'$, where $\Delta'\equiv k_{zs}'+k_{zi}'$. After integration over ξ_1,ξ_2, there will be a term in Eq. (23) like

$$\exp\{-2\sigma^2(1-C^2)[(\Delta')^2-(k_{zs}''\pm k_z'')^2]\}\ , \tag{25}$$

where $C \equiv \langle \xi_1 \xi_2 \rangle / \sigma^2$ is the normalized correlation function and σ^2 is the variance. As the observation moves away from the backscattering direction, $\Delta' = k'_{zs} + k'_{2i} \gg k''_z$. Thus, the bistatic scattering $\gamma_s^{(2-)}$ of the second average of Eq. (13) will be negligible comparing with $\gamma_s^{(2+)}$ of the first one. However, as the observation moves closer to the backscattering direction, Δ' approaches zero, the difference between $\gamma_s^{(2+)}$ and $\gamma_s^{(2-)}$ is diminished, and $\gamma_s^{(2-)}$ increases and reaches its maximum value, when $\Delta' = 0$ (in the backscattering direction). This contribution causes the scattering enhancement around the backscattering direction.

For simplicity, the correlation between heights (ξ_1, ξ_2) and slopes $(\bar{\alpha}_{10}, \bar{\alpha}_{20})$ is now omitted, i.e.,

$$p_6(\xi_1, \xi_2, \bar{\alpha}_{10}, \bar{\alpha}_{20}) \approx p_2(\xi_1, \xi_2) p_4(\bar{\alpha}_{10}, \bar{\alpha}_{20}) .$$

Thus, we consider herewith the integrations over ξ_1 and ξ_2 in Eqs. (20) and (23) in

$$I^{(+)} = \int_{-\infty}^{\infty} d\xi_1 \int_{-\infty}^{\infty} d\xi_2 p_2(\xi_1, \xi_2) \exp[2(k''_{zs} \mp k''_z)\xi_2] \times \exp[-2(k''_{zi} \mp k''_z)\xi_1] , \quad (26a)$$

$$I^{(-)} = \int_{-\infty}^{\infty} d\xi_1 \int_{-\infty}^{\infty} d\xi_2 p_2(\xi_1, \xi_2) \times \exp[2(k''_{zs} \mp k''_z \mp i\Delta')\xi_2] \times \exp[-2(k''_{zi} \mp k''_z \mp i\Delta')\xi_1] . \quad (26b)$$

Assume that the roughness distribution is a Gaussian

$$p_2(\xi_1, \xi_2) = \frac{1}{2\pi\sigma^2(1-C^2)^{1/2}} \exp(-a_0\xi_1^2 - c_0\xi_1\xi_2 - a_0\xi_2^2) , \quad (27a)$$

where

$$a_0 = \frac{1}{2\sigma^2(1-C^2)}, \quad c_0 = -\frac{C}{\sigma^2(1-C^2)}, \quad C = e^{-\rho^2/l^2} , \quad (27b)$$

where l is the correlation length.

Substituting (27) into (26b), and integrating over ξ_2 ($\xi_2 \geq \xi_1$, denoting u, upgoing), we obtain

$$I^{(-)u} = \frac{1}{2\sqrt{\pi}} \exp\{-2\sigma^2(1-C^2)[(\Delta')^2 - (k''_{zs} - k''_z)^2]\} \exp[-i4\sigma^2(1-C^2)\Delta'(k''_{zs} - k''_z)] \times \int_{-\infty}^{\infty} d\frac{\xi_1}{\sqrt{2}\sigma} \exp\left[-\frac{\xi_1^2}{2\sigma^2} + 2[(1-C)(i\Delta' + k''_z) - (k''_{zi} - Ck''_{zs})]\xi_1\right] \times \operatorname{erfc}\left[\frac{\xi_1}{\sqrt{2}\sigma}\sqrt{(1-C)/(1+C)} - \sqrt{2}\sigma(1-C^2)^{1/2}(k''_{zs} - k''_z - i\Delta')\right] \quad (28a)$$

and for $\xi_2 < \xi_1$ (denoting d, downgoing),

$$I^{(-)d} = \frac{1}{2\sqrt{\pi}} \exp\{-2\sigma^2(1-C^2)[(\Delta')^2 - (k''_{zs} + k''_z)^2]\} \exp[i4\sigma^2(1-C^2)\Delta'(k''_{zs} + k''_z)] \times \int_{-\infty}^{\infty} d\frac{\xi_1}{\sqrt{2}\sigma} \exp\left[-\frac{\xi_1^2}{2\sigma^2} - 2[(1-C)(i\Delta' + k''_z) + (k''_{zi} - Ck''_{zs})]\xi_1\right] \times \left[2 - \operatorname{erfc}\left[\frac{\xi_1}{\sqrt{2}\sigma}\sqrt{(1-C)/(1+C)} - \sqrt{2}\sigma(1-C^2)^{1/2}(k''_{zs} + k''_z + i\Delta')\right]\right] . \quad (28b)$$

$I^{(+)}$ of Eq. (26a) simply follows from Eq. (28) by setting $\Delta' = 0$.

We can see that when $\Delta' \gg k''_{zs} \pm k''_z$, $I^{(-)}$ is much less than $I^{(+)}$ due to exponential decay. When one approaches the backscattering direction, $0 \leftarrow \Delta' \approx k''_{zs} \pm k''_z$, $I^{(-)}$ approaches $I^{(+)}$. This produces the enhancement. The angular width of the enhancement depends upon the factor from Eq. (25):

$$\exp\{-2(2\pi\sigma/\lambda)^2(1-C^2)[(\cos\theta_s - \cos\theta_i)^2 - (k''|k')^2(1/\cos\theta_s \pm 1/\cos\theta)^2]\} . \quad (29)$$

The shadowing function $S(\hat{\mathbf{k}}, \bar{\alpha}_{10}, \bar{\alpha}_{20})$ takes account of any shadowing in the scattering between ξ_1 and ξ_2. It depends on the slopes, heights of the correlated points $\mathbf{r}_1$ and $\mathbf{r}_2$, and the distance between them. It is a complicated function,[31] and requires integration over all possible ξ_1, ξ_2. Since we further approximate $C \approx 0$, the dependence of C on $\bar{\rho}$ disappears. This approximation is equivalent to neglecting correlation between the heights at separate stationary points, $\mathbf{r}_1$ and $\mathbf{r}_2$. This assumption, valid when the correlation length is less than the average separation between stationary phase points, is not part of our basic theory but is used to facilitate obtaining an explicit analytic answer. We intuitively take the shadowing function to be

$$S(\hat{\mathbf{k}}, \bar{\alpha}_{10}, \bar{\alpha}_{20}) = \Theta(\cot\theta - \alpha_1, \alpha_2 - \cot\theta)\cos\theta_s \times \exp[-(2\sqrt{2}\sigma/l)\tan\theta(\rho/l)] , \quad (30a)$$

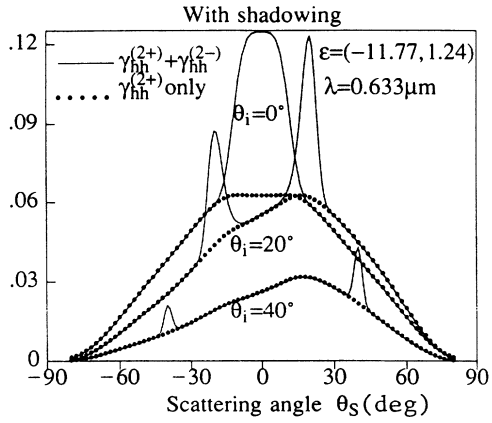

FIG. 4. Double scattering vs scattering angle with Wagner shadowing, showing forward and backward enhancement. Parameters are the same as in Fig. 2.

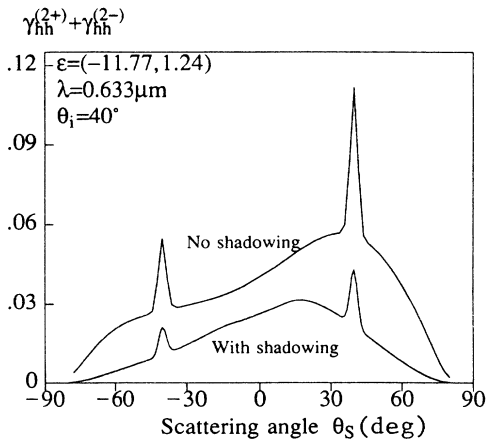

FIG. 5. Double scattering showing forward and backward enhancement vs scattering angle. A comparison is made at 40° between the presence and absence of Wagner shadowing.

where $\sqrt{2}\sigma/l$ is the mean-square-root slope, and the function

$$\Theta(x,y)=\begin{cases}1 & \text{as } x \text{ and } y>0\\ 0 & \text{otherwise}\end{cases} \tag{30b}$$

(where $\alpha_1\equiv\alpha_{1x}\cos\phi+\alpha_{1y}\sin\phi$ $\alpha_2\equiv\alpha_{2x}\cos\phi+\alpha_{2y}\sin\phi$) takes account of the self-shadowing effect. The shadowing function of Eq. (30a) can be understood that at $\cot\theta=\sqrt{2}\sigma/l$ and $\rho=l$, the shadowing function is approximately 0.1; as θ or $\rho/l\to 0$, the shadowing function approaches 1 (no shadowing), and

$$S(\hat{\mathbf{k}}_i,\bar{\boldsymbol{\alpha}}_{10})S(\hat{\mathbf{k}}_s,\bar{\boldsymbol{\alpha}}_{20})\approx S(\hat{\mathbf{k}}_i,\hat{\mathbf{k}}_s) \tag{30c}$$

is taken as in Ref. 20. Substituting (28) and (30) into (23) or (24), we obtain

$$\begin{aligned}\gamma_{pq}^{(2-)}=\frac{\pi\cos^2\theta_{0i}}{\cos\theta_s}\int_0^{\pi/2}d\theta\int_0^{2\pi}d\phi\frac{1}{2\sqrt{2}\sigma}p_4(\bar{\boldsymbol{\alpha}}_{10},\bar{\boldsymbol{\alpha}}_{20})S(\hat{\mathbf{k}}_i,\hat{\mathbf{k}}_s)\\ \times\{F_{pq}(\mathbf{k}_s,\mathbf{k}_\rho+k_z\hat{\mathbf{z}},\mathbf{k}_i)F_{pq}^*(\mathbf{k}_s,\mathbf{k}_{1\rho}+k_{1z}\hat{\mathbf{z}},\mathbf{k}_i)\cos[4\sigma^2\Delta'(k_{zs}''+k_{zi}''-2k_z'')]\\ \times\tfrac{1}{2}\exp\{-2\sigma^2[(\Delta')^2-(k_{zs}''-k_z'')^2]\}\exp\{-2\sigma^2[(\Delta')^2-(k_{zi}''-k_z'')^2]\}\\ +F_{pq}(\mathbf{k}_s,\mathbf{k}_\rho-k_z\hat{\mathbf{z}},\mathbf{k}_i)F_{pq}^*(\mathbf{k}_s,\mathbf{k}_{1\rho}-k_{1z}\hat{\mathbf{z}},\mathbf{k}_i)\cos[4\sigma^2\Delta'(k_{2z}''+k_{zi}''+2k_z'')]\\ \times\tfrac{1}{2}\exp\{-2\sigma^2[(\Delta')^2-(k_{zs}''+k_z'')^2]\}\exp\{-2\sigma^2[(\Delta')^2-(k_{zi}''+k_z'')^2]\}\}\,.\end{aligned} \tag{31}$$

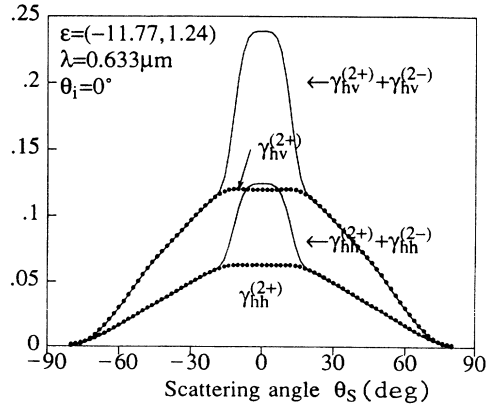

FIG. 6. Double-scattering enhancement at normal incidence. Parameters are those used in Fig. 2.

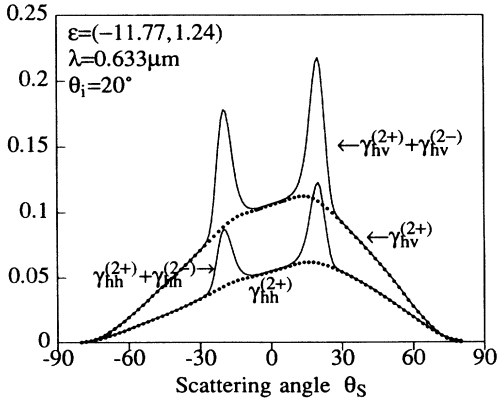

FIG. 7. Double-scattering enhancement at 20° incidence. Forward and backward peaks visible at ±20°. Parameters are those used in Fig. 2.

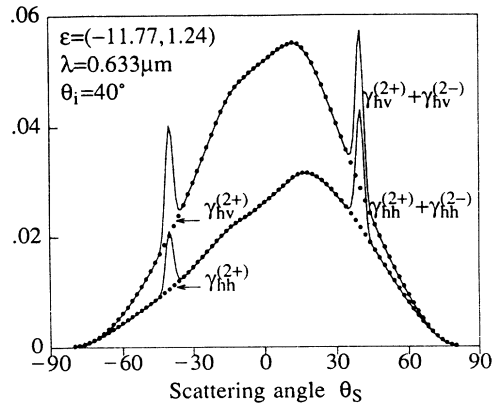

FIG. 8. Double-scattering enhancement at 40° incidence. Forward and backward peaks visible at ±40°. Parameters are those used in Fig. 2.

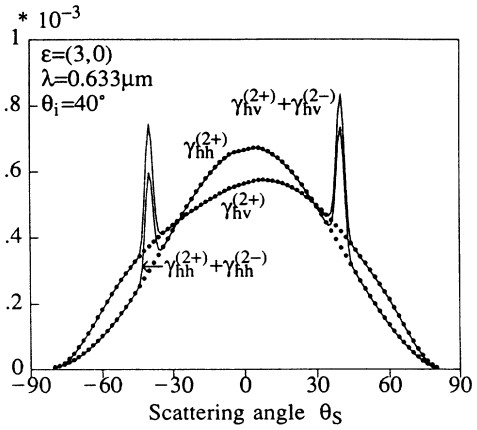

FIG. 10. Double scattering at $\theta_i = 40°$ incidence to a dielectric surface. Parameters ares are same as in Fig. 9, except for incidence angle.

$\gamma^{(2+)}$ simply follows from Eq. (31) by setting $\Delta' = 0$.

V. NUMERICAL RESULTS

Numerical calculations for single-scattering $\gamma_{pq}^{(1)}$ of Eq. (11), were displayed in Eqs. (2) and (3). The double-scattering $\gamma_{pq}^{(2+)}$ and $\gamma_{pq}^{(2-)}$ of Eqs. (16b) and (24) are obtained, and are shown in Figs. 4–11, respectively.

From Eq. (29), we see that the width W of the enhancement lines varies as

$$W \approx \frac{\lambda}{\sigma \sin\theta_s} . \tag{32}$$

The decrease of width as the angle of incident (or scattering) increases is shown clearly in Fig. 4. The width decreases markedly as the incident angle increases from 0° to 20° and 40°. Figure 5 shows a comparison at 40° between scattering with and without the inclusion of scattering effects. Two points are clear: The effect of shadowing is appreciable, but it does not modify the width of the enhancement peaks.

Figures 6–8 demonstrate that the enhancement peaks are definitely due to the reversed path included in γ^{2-}. They also show that the peaks for the case of a polarization change (hv) are comparable to those (hh) that have no polarization change.

Figures 9 and 10 show that the enhanced peak can occur in the case of dielectric reflection as opposed to the metallic reflection considered earlier.

Figures 11 and 12 show that an enhancement occurs at the longer wavelength of 10 μm, but as expected from Eq. (40) the linewidth has increased significantly with the increase in wavelength. The results displayed in the above figures are quite consistent with the available experimental observations.[5]

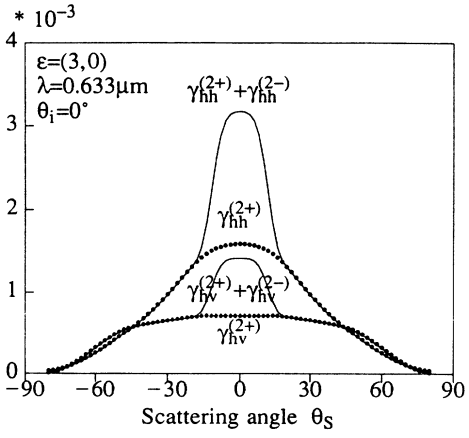

FIG. 9. Double-scattering enhancement at normal incidence to a dielectric surface A forward or backward peak produced by the reversed path contribution is clearly visible. Parameters are those used in Fig. 2 except the dielectric constant, which has been set to $\epsilon = (3,0)$.

VI. CONCLUSION

Upon employing the Kirchhoff approach, an analytic formula of polarized bistatic double-scattering intensity is

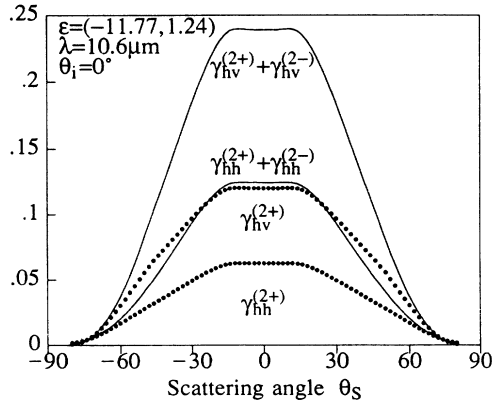

FIG. 11. Double-scattering enhancement at normal incidence. A forward or backward peak produced by the reversed path contribution is clearly visible. Parameters are those used in Fig. 2 except the wavelength has been set to 10.6 μm.

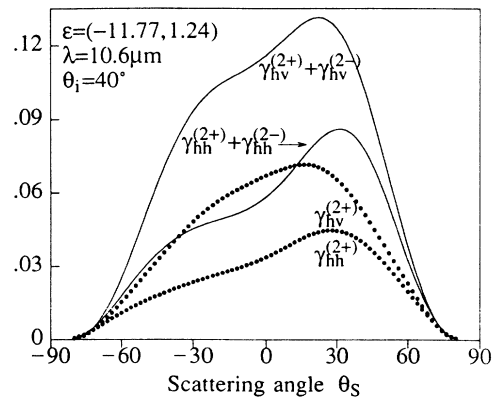

FIG. 12 Double-scattering enhancement at normal incidence. A forward or backward peak produced by the reversed path contribution is clearly visible. Parameters are those used in Fig. 11 except the angle of incidence has been set to $\theta=40°$.

obtained. This formula contains the contributions from constructive interference of the coincidental and anticoincidental waves from a rough surface. The behavior of the latter causes an angular enhancement around the backscattering direction, since its change depends upon $k'_{sz}+k'_{iz}$ in comparison with k''_z. It takes a maximum as $k'_{sz}+k'_{iz}=0$ at the backscattering direction, and becomes negligible as $k'_{sz}+k'_{iz}\gg k''_z$. The angular distribution of the enhancement depends upon $\sigma/\lambda, \sigma/l$, incident θ_i, the underlying medium dielectric constant ϵ_1, and some other parameters (e.g., k''/k'). Incorporating an approximate shadowing function, this formula is used to evaluate the scattering enhancement and bistatic double-scattering from rough surfaces. The results are consistent with the observations.

ACKNOWLEDGMENTS

This work was supported by the Chemical Research Development and Engineering Center (Aberdeen Proving Ground), the U.S. Army Research Office and the U.S. Department of Energy. We are indebted to Ms. R. C. Fulton for repeating the calculations with higher resolution, checking the code, and generating additional figures.

APPENDIX A

We say

$$F_{hh}^{(d)}=M_d[(\hat{\mathbf{v}}_b\cdot\hat{\mathbf{k}}_\alpha)(\hat{\mathbf{v}}_a\cdot\hat{\mathbf{k}}_b)R_{hd}+(\hat{\mathbf{h}}_b\cdot\hat{\mathbf{k}}_a)(\hat{\mathbf{h}}_a\cdot\hat{\mathbf{k}}_b)R_{vd}] ,$$
$$F_{hv}^{(d)}=M_d[(\hat{\mathbf{h}}_b\cdot\hat{\mathbf{k}}_a)(\hat{\mathbf{v}}_a\cdot\hat{\mathbf{k}}_b)R_{hd}-(\hat{\mathbf{v}}_b\cdot\hat{\mathbf{k}}_a)(\hat{\mathbf{h}}_a\cdot\hat{\mathbf{k}}_b)R_{vd}] ,$$
$$F_{vh}^{(d)}=M_d[(\hat{\mathbf{v}}_b\cdot\hat{\mathbf{k}}_a)(\hat{\mathbf{h}}_a\cdot\hat{\mathbf{k}}_b)R_{hd}-(\hat{\mathbf{h}}_b\cdot\hat{\mathbf{k}}_a)(\hat{\mathbf{v}}_a\cdot\hat{\mathbf{k}}_b)R_{vd}] ,$$
$$F_{vv}^{(d)}=M_d[(\hat{\mathbf{h}}_b\cdot\hat{\mathbf{k}}_a)(\hat{\mathbf{h}}_a\cdot\hat{\mathbf{k}}_b)R_{hd}+(\hat{\mathbf{v}}_b\cdot\hat{\mathbf{k}}_a)(\hat{\mathbf{v}}_a\cdot\hat{\mathbf{k}}_b)R_{vd}] ,$$

where the parameters d,a,b are

$d=0$,
$a=i$ for Eqs. (11), (17), and (18),
$b=s$,

$$\begin{aligned} &d=1+ ,\\ &a=i ,\\ &b=1,\ \hat{\mathbf{k}}_1\equiv\hat{\mathbf{k}} , \end{aligned} \quad \text{and} \quad \begin{cases} d=1-,\\ a=i ,\\ b=1,\hat{\mathbf{k}}_1\equiv\hat{\mathbf{k}}_i+\hat{\mathbf{k}}_s-\hat{\mathbf{k}} , \end{cases}$$

$$\begin{aligned} &d=2+ ,\\ &a=1,\ \hat{\mathbf{k}}_1\equiv\hat{\mathbf{k}} ,\\ &b=s, \end{aligned} \quad \text{and} \quad \begin{cases} d=2- ,\\ a=1 ,\hat{\mathbf{k}}_1\equiv\hat{\mathbf{k}}_i+\hat{\mathbf{k}}_s-\hat{\mathbf{k}} ,\\ b=s , \end{cases}$$

$$M_d=\frac{|\delta\mathbf{k}_d|^2}{k|\hat{\mathbf{k}}_a\times\hat{\mathbf{k}}_b|^2\delta k_{dz}} ,$$

where

$$\delta\mathbf{k}_{1+}\equiv\mathbf{k}_i-\mathbf{k},\ \delta\mathbf{k}_{1-}\equiv\mathbf{k}-\mathbf{k}_s ,$$
$$\delta\mathbf{k}_{2+}\equiv\mathbf{k}-\mathbf{k}_s,\ \delta\mathbf{k}_{2-}\equiv\mathbf{k}_i-k ,$$

and the local Fresnel reflection coefficients are

$$R_{hd}=\frac{\cos\theta_{ld}-(\epsilon_{1n}-\sin^2\theta_{ld})^{1/2}}{\cos\theta_{ld}+(\epsilon_{1n}-\sin^2\theta_{ld})^{1/2}} ,$$
$$R_{vd}=\frac{\epsilon_{1n}\cos\theta_{ld}-(\epsilon_{1n}-\sin^2\theta_{ld})^{1/2}}{\epsilon_{1n}\cos\theta_{ld}+(\epsilon_{1n}-\sin^2\theta_{ld})^{1/2}} ,$$
$$\epsilon_{1n}\equiv\epsilon_1/\epsilon_0 .$$

The local angle $\cos\theta_{ld}=-\hat{\mathbf{n}}\cdot\hat{\mathbf{k}}_a$, where $\hat{\mathbf{n}}$ is the stationary slope at the point ξ_1 or ξ_2, respectively.

APPENDIX B

We can estimate the area parameter S of Eq. (13) by comparing our exact results, Eq. (11) for single-scattering with an approximation of the same sort; see Eq. (13b) as was used in the double-scattering case.

If Eq. (9a) is squared and Eq. (9d) is introduced, we obtain

$$|\mathbf{E}_s^{(1)}(\mathbf{r})|^2/|\mathbf{E}_0|^2=|M|^2 ,$$

where

$$|M|^2=k^2\left|\int d\boldsymbol{\rho}_1\vec{\mathbf{g}}(\mathbf{r},\mathbf{r}_1)\cdot\vec{\mathbf{R}}_0(k_s,k_i)\cdot\mathbf{e}_i\exp(ikr_1)\right|^2 . \quad \text{(B1)}$$

If the approximation, Eq. (13b) is made, the fourfold integration of Eq. (B2) is reduced to the twofold integral:

$$|M|^2=k^2S\int d\boldsymbol{\rho}_1|\vec{\mathbf{g}}(\mathbf{r},\mathbf{r}_1)\cdot\vec{\mathbf{R}}_0\cdot\mathbf{e}_i|^2 . \quad \text{(B2)}$$

If the integral representation Eq. (14a) is introduced for the Green's function the integration over $\boldsymbol{\rho}_1$ yields a δ function

$$(2\pi)^2\delta(\mathbf{k}'_\rho-\mathbf{k}_\rho) .$$

The result is that

$$|M|^2=\int d\mathbf{k}_\rho f(\mathbf{k}_\rho) , \tag{B3}$$

where the electric field spectrum of Eq. (16c) is given by

$$f(\mathbf{k}_\rho)=k^2S(2\pi)^2|\vec{\mathbf{g}}(\mathbf{k}_\rho,z,z_1)\cdot\vec{\mathbf{R}}_0\cdot\mathbf{e}_i|^2 . \tag{B4}$$

Introducing the expression, Eq. (14) for the Green's function in $\mathbf{k}$ space, we can write

$$f(\mathbf{k}_\rho)=\frac{k^2}{(k_z)^2}\frac{S}{(4\pi)^2}|\langle\mathbf{b}|\vec{\mathbf{R}}_0|\mathbf{a}\rangle|^2 , \tag{B5}$$

where we have written $\mathbf{a}$ for the input polarization vector $\mathbf{e}_i$ and $\mathbf{b}$ for the polarization of the scattered light.

If we make use of Eq. (11a) the bistatic cross section is given by

$$\gamma_{ba}=\frac{k^2|\langle\mathbf{b}|\vec{\mathbf{R}}_0|\mathbf{a}\rangle|^2}{4\pi}\frac{k^2S\cos^2\theta_i}{k_{sz}^2} . \tag{B6}$$

Comparison between this approximation procedure, and the better one used in Sec. II, Eq. (11e), permits the following crude estimate of the area S:

$$k^2S=\frac{1}{4}\frac{\cos^2\theta_s}{\cos^3\theta_i}k^2\frac{\langle|I|^2\rangle}{A} , \tag{B7}$$

where the last factor is given in Eq. (11c).

*Present address: Department of Electronic Engineering, Fudan University, Shanghai 20033, People's Republic of China.

[1]F. Becker, P. Ramanantsizehena, and M. Stoll, Appl. Opt. **24**, 365 (1985).
[2]E. R. Mendez and K. A. O'Donnell, Opt. Commun. **61**, 91 (1987).
[3]A. R. McGurn, A. A. Maradudin, and V. Celli, Phys. Rev. B **30**, 3136 (1984); **31**, 4866 (1985).
[4]V. Celli, A. A. Maradudin, A. M. Marvin, and A. R. McGurn, J. Opt. Soc. Am. A **2**, 2225 (1985).
[5]K. A. O'Donnell and E. R. Mendez, J. Opt. Soc. Am. A **4**, 1194 (1987).
[6]P. Beckmann and A. Spizzichino, *The Scattering of Electromagnetic Waves From Rough Surfaces* (Pergamon, New York, 1963).
[7]F. G. Bass and I. M. Fuks, *Wave Scattering From Statistically Rough Surfaces* (Pergamon, New York, 1979).
[8]D. A. de Wolf, IEEE Trans. Antennas Prop. **AP-19**, 254 (1971).
[9]J. A. DeSanto, J. Math. Phys. **27**, 377 (1986).
[10]G. S. Brown, IEEE Trans. Antennas Prop. **AP-32**, 1308 (1984).
[11]G. S. Brown, IEEE Trans. Antennas Prop. **AP-33**, 48 (1985).
[12]M. Nieto-Vesperinas and J. M. Soto-Crespo, Opt. Lett. **12**, 979 (1987).
[13]A. A. Maradudin, E. R. Meńdes, and T. Michel, Opt. Lett. **14**, 151 (1988).
[14]A. A. Mardudin, E. R. Meńdes, and T. Michel, in *Scattering in Volumes and Surfaces,* edited by M. Nieto-Vesperinas and J. M. Soto-Crespo (North-Holland, Amsterdam, 1990), p. 157.
[15]P. Tran and V. Celli, J. Opt. Soc. Am. A **5**, 1635 (1988).
[16]For a review, see P. A. Lee and T. V. Ramakrishnan, Rev. Mod. Phys. **57**, 287 (1985).
[17]Proposals that photon localization can also be achieved are given by K. Arya, Z. B. Su, and J. L. Birman, Phys. Rev. Lett. **57**, 2725 (1986); **54**, 1559 (1985).
[18]Jin Au Kong, *Electromagnetic Wave Theory* (Wiley, New York, 1986).
[19]A. Stogryn, Radio Sci. (New Series) **2**, 415 (1967).
[20]M. I. Sancer, IEEE Trans. Antennas Prop. **AP-17**, 577 (1969).
[21]R. J. Wagner, J. Acoust. Soc. Am. **41**, 138 (1967).
[22]R. A. Brockelman and T. Hagfors, IEEE Trans. Antennas Prop. **AP-14**, 621 (1966).
[23]P. Beckmann, IEEE Trans. Antennas Prop. **AP-14**, 626 (1966). This is a discussion of Ref. 22.
[24]B. G. Smith, IEEE Trans. Antennas Prop. **AP-15**, 668 (1967); J. Geophys. Res. **72**, 4059 (1967).
[25]Y. Q. Jin and J. A. Kong, J. Math. Phys. **26**, 994 (1986).
[26]See F. G. Bass and I. M. Fuks, *Wave Scattering from Statistically Rough Surfaces,* Ref. 7, p. 12.
[27]M. Lax, Rev. Mod. Phys. **23**, 287 (1951).
[28]A. K. Fung and H. S. Fung, IEEE Trans. Geosci. Electron. **GE-15**, 189 (1977).
[29]A. Zumiga and J. A. Kong, J. Appl. Phys. **51**, 74 (1981).
[30]S. T. Wu and A. K. Fung, J. Geophys. Res. **77**, 5917 (1972).
[31]Y. Q. Jin, J. Appl. Phys. **63**, 1286 (1988).